Journal of
Composites Science

MDPI

Article

Carbon Nanoparticle-Loaded PLA Nanofibers via Electrospinning for Food Packaging

Pietro Di Matteo [1], Francesco Barbero [2], Enrique Giménez-Torres [3], Ivana Fenoglio [2], Elena Destro [2], Valentina Brunella [1,*] and Águeda Sonseca Olalla [3,*]

[1] Department of Chemistry, Università di Torino, 10125 Turin, Italy; pietro.dimatteo@unito.it
[2] Department of Chemistry and Interdepartmental Centre for Nanostructured Interfaces and Surfaces, Università di Torino, 10125 Turin, Italy; francesco.barbero@unito.it (F.B.); ivana.fenoglio@unito.it (I.F.); elena.destro@unito.it (E.D.)
[3] Instituto Universitario de Investigación de Tecnología de los Materiales, Universitat Politécnica de Valéncia, UPV, 46022 Valencia, Spain; enrique.gimenez@mcm.upv.es
* Correspondence: valentina.brunella@unito.it (V.B.); agsonol@upvnet.upv.es (Á.S.O.)

Abstract: The development of nanocomposite materials for food packaging applications requires a precise balance of material functionality, safety, and regulatory compliance. In this work, the design, manufacturing, optimization, feasibility, and safety profile of polylactic acid (PLA) nanofibers filled with biocompatible carbon nanoparticles (CNP) and copper-loaded (CNP-Cu) nanoparticles by electrospinning are presented. To ensure nanoparticle compatibility with the PLA solvent system and achieve a uniform dispersion of the nanoparticles within nanofibers, dynamic light scattering analysis was employed, while the incorporation efficiency was demonstrated by building a novel UV–vis spectroscopy analytical method. Morphological analysis, performed through FE-SEM and TEM, confirmed the homogeneous distribution of CNP and CNP-Cu nanoparticles without aggregation. Migration studies in aqueous food simulants were also carried out to assess the material's safety profile. The results showed minimal nanoparticle release, and the calculated copper migration was well within the limits set by European Commission Regulation (EU) No. 10/2011 for food contact materials.

Keywords: carbon nanoparticles; copper; polylactic acid; electrospinning; manufacturing; food packaging

Academic Editor: Traian Dumitrica

Received: 21 November 2024
Revised: 20 December 2024
Accepted: 30 December 2024
Published: 7 January 2025

Citation: Di Matteo, P.; Barbero, F.; Giménez-Torres, E.; Fenoglio, I.; Destro, E.; Brunella, V.; Sonseca Olalla, Á. Carbon Nanoparticle-Loaded PLA Nanofibers via Electrospinning for Food Packaging. *J. Compos. Sci.* **2025**, *9*, 25. https://doi.org/10.3390/jcs9010025

1. Introduction

The development of advanced materials for food packaging is a growing priority in both the scientific and industrial sectors because of the need for safer and more functional packaging systems [1].

In recent years, nanotechnology has been widely used to explore novel alternatives to enhance food packaging, using various active agents as material fillers to improve its properties [2–4].

Several nanoparticles have been proposed, with metals and metal oxides such as silver, zinc oxide, and copper oxide being among the most studied [5,6]. In addition, carbon-based nanomaterials, including carbon nanotubes, graphene, and carbon dots, have gained attention for their versatile properties and potential applications in the food industry and beyond [7–9].

However, even with the promising capabilities of these nanofillers, one of the primary issues associated with their usage is the possible migration into food products [10], posing risks to both human health and the environment [6].

In this scenario, hydrothermal carbon-based nanoparticles (CNPs) are of particular interest. This kind of nanomaterial is produced through the hydrothermal carbonization of saccharides, a green synthetic method, leading to spherical particles with defined sizes.

Previously, we reported that CNPs are an efficacious and biocompatible [11] nano-delivery system for antimicrobial agents such as peptides and copper [12].

Polymers derived from renewable resources are classified as bio-derived polymers [13]. Among these, polylactic acid (PLA) stands out for its biocompatibility, mechanical properties, and processability [14,15]. Moreover, its non-toxic nature [16] holds promise for different applications, especially in the food and beverage industries [17–20].

PLA-based packaging materials have been processed by different conventional fabrication technologies such as extrusion [21], injection molding [22], and thermoforming [14]. In addition, it has been processed as a nanostructured material by means of non-conventional techniques such as electrospinning [23–25]. This versatile, cost-effective, and scalable technique is emerging as a powerful method to fabricate nanofibrous materials with controlled morphology [26]. It allows the production of fibers with high surface area-to-volume ratios and with diameters from nanometres to micrometres, significantly enhancing moisture and oxygen barrier properties [27]. Furthermore, PLA nanofibers exhibit improved mechanical properties [28] such as increased strength, flexibility, and toughness compared to bulk PLA. Moreover, these fibers can be functionalized with antimicrobial agents, nanoparticles [29,30], or other bioactive compounds [31], providing active packaging solutions that help to inhibit microbial growth [32]. Considering these advantages, electrospinning was selected to incorporate CNP and copper-loaded CNP (CNP-Cu) into PLA nanofibers.

Finally, this work describes an efficient method to encapsulate CNP and CNP-Cu into PLA nanofibers via electrospinning, leveraging electrospinning ability to improve the dispersion of fillers [29] and the possibility of controlling the fibers' diameter and porosity and offering the potential of enhancing the material's antimicrobial properties while ensuring compliance with European Commission Regulation (EU) No 10/2011 [33], which governs the safety of materials intended to come into contact with food.

2. Materials and Methods

Polylactic acid (PLA Polymer 3051D) pellets were sourced from NatureWorks®, LLC, Minnetonka, MN, USA. It is a semicrystalline polymer consisting of 96% L- and 4% D-lactide monomers with a molecular weight (M_n) of 1.62×10^4 g mol^{-1}. Its density (d) is 1.24 g/cm^3, while the glass transition temperature (T_g) is 55–65 °C and the melting temperature is 150–165 °C [34]. Both dichloromethane (DCM) and N-N dimethylformamide (DMF) solvents were supplied by Scharlau, Aquagent®; Solvent, Barcelona, Spain, and used as received.

Prior to use, PLA pellets were dried at 60 °C for 12 h in an oven: this procedure prevents moisture absorption, which can affect PLA's properties [35,36].

Carbon nanoparticles were synthesized according to the hydrothermal carbonization method described by Scattareggia et al. [12]. Glucose was dissolved in ultrapure water and sodium polyacrylate was added to prevent crosslinking. The solution was magnetically stirred, transferred to a Teflon-lined stainless-steel autoclave (Büchi AG, Uster, Switzerland), and heated at 190 °C with specific durations to produce two sizes of CNPs, small (SCNP) and large (LCNP), resulting in a mean Feret's diameter of 88 ± 22 nm and 242 ± 86 nm, respectively. CNP suspensions were then purified through ultrafiltration.

Copper loading onto nanoparticles was achieved by incubating the CNP suspension in $CuSO_4$ aqueous solution, followed by centrifugation to remove excess metal ions.

In this work, we specifically utilized LCNP (CNP) and copper-loaded LCNP-Cu (CNP-Cu).

2.1. Characterization of Carbon Nanoparticles

2.1.1. ζ-Potential of Pristine Nanoparticles and Copper-Loaded Nanoparticles

Electrophoretic light scattering (ELS) was performed using a Zetasizer (Nano ZS, Malvern Instruments, Malvern, Worcestershire, UK) to measure the ζ-potential of CNP and CNP-Cu suspensions. Following the methodology described by Fenoglio Ivana, et al. [37], samples were diluted 1:200 in self-produced ultrapure Milli-Q water (pH 5.05 and conductivity 0.08 mS/cm), with the following parameters: refractive index = 2.417 and absorption = 1.00.

The results were expressed as mean values of three independent measurements ± standard deviation.

2.1.2. Quantification of Copper Content in CNP-Cu

The copper ion content in the CNP-Cu sample was quantified using Inductively Coupled Plasma Optical Emission Spectroscopy (ICP-OES) with a PerkinElmer Optima 2000 DV instrument (Norwalk, CT, USA). For the analysis, 5 mL of each CNP suspension was placed in high-pressure Teflon bombs, followed by the addition of 1 mL of hydrogen peroxide (H_2O_2, 30% w/w) and 4 mL of nitric acid (HNO_3, 65%). The samples underwent digestion using a Microwave Digestion System (Milestone Microwave MLS 1200 Mega, Sorisole, Italy) under the following program: 1 min at 250 W, 2 min pause, 5 min at 200 W, 5 min at 350 W, 5 min at 550 W, 5 min at 250 W, and 10 min for cooling.

2.2. NEAT PLA Electrospinning

The PLA solutions were prepared by dissolving PLA in a 70:30 v/v DCM–DMF solvent system to achieve concentrations of 7, 8.5, 9, and 10 wt.%. This solvent system has been demonstrated to provide optimal viscosity for electrospinning similar PLA concentrations [38].

The density of the final solution was determined using a Gay-Lussac Pycnometer (BLAUBRAND®, Wertheim, Germany) in accordance with DIN 12797 standards [39]. A total of 9.26 g of DCM (d = 1.32 g/cm^3) and 2.82 g of DMF (d = 0.94 g/cm^3) were used. The pycnometer was calibrated and used at a controlled temperature to minimize thermal expansion effects on the density calculation. The mass of the solution in the instrument was measured with an analytical balance, and the known volume of the pycnometer was used to calculate the density of the solution (d = 1.212 g/cm^3).

Initially, the DCM–DMF mixture was prepared, followed by the addition of PLA at the various concentrations. The resulting solutions were magnetically stirred at room temperature for 3 h until complete dissolution.

For the manufacturing process, a Nanofiber Electrospinning unit (ESpin Nanotech, SUPER ES-2, Kanpur, Uttar Pradesh, India), equipped with a metal rotating drum collector and a syringe pump system, was used. Once prepared, the solution was pumped into a stainless-steel needle from the syringe and tested with the following setup conditions: flow rate = 2.0 mL/h, voltage =15 kV, and working distance = 11 cm. The final mats were obtained after 2 h under controlled conditions of relative humidity (RH) of less than 50% and finally collected on aluminum foil wrapped around the metallic collector.

The most promising PLA concentration was tested with four different spinning setups to optimize the instrument parameters and enhance the evaporation of the solvent and Taylor cone formation. The different setups were tested with flow rates, voltages, and working distances between 1.5–2.5 mL/h, 15–20 kV, and 11–13 cm, respectively.

2.3. Dynamic Light Scattering

A Zetasizer (Nano ZS Malvern Instruments, Malvern, Worcestershire, UK) instrument was used to evaluate the CNP aggregation state at 1 wt.% in both individual solvents, DCM and DMF, and in their 70:30 v/v mixture, before and after sonication (120 W, 50/60 Hz bath). Once prepared, the suspensions were transferred to a quartz cuvette for analysis.

It has been demonstrated in the literature that PLA can be effectively dissolved in a 70:30 v/v DCM–DMF solution [38]. DCM typically serves as an excellent solvent due to its ability to break PLA's crystalline structure [23] while DMF stabilizes the solution, preventing rapid evaporation and favouring the spinning process [40]. Given these premises, dynamic light scattering (DLS) analyses were used to study nanoparticles' dispersibility in solvents in comparison to aqueous environments, where appropriate results have already been documented [12].

2.4. Nanocomposite Electrospinning

Nanocomposite mats were obtained using 1.0 wt.% CNP and CNP-Cu fillers.

Initially, both CNP and CNP-Cu were dispersed in 1.32 g of DMF and sonicated for 30 min (sonication bath 120 W, 50/60 Hz) as determined from DLS analysis. Concurrently, 1.0 g of the PLA pellet was mixed with 9.26 g of DCM and 1.5 g of the DMF solution and stirred until complete dissolution.

Once homogeneous dispersions of CNP and CNP-Cu were achieved in DMF, and the PLA pellet was fully dissolved in the solvent system, the solutions were mixed, obtaining a final solution with 10 wt.% PLA in 70:30 v/v DCM–DMF and 1 wt.% of CNP and CNP-Cu, respectively (CNP percentages were relative to the initial PLA wt.%).

Finally, electrospinning (unit system described for neat PLA) was used to manufacture nanocomposites using the optimized setup parameters achieved for PLA fiber production.

Mats were obtained over 2 h under controlled conditions (RH < 50%) and collected on aluminum foil around the collector.

2.5. Quantification of CNP Concentration in PLA Mats

A novel method was employed to quantify the concentration of carbon nanoparticles (CNPs) in the electrospun mats using UV–Vis spectrophotometry. A UVICON 930 spectrophotometer (Kontron Instruments, Basel, Switzerland), equipped with both halogen and tungsten lamps, covering a spectral range from 850 to 190 nm, was used. The method served to verify that the initial CNP concentration in solution was effectively retained in the final nanocomposite mat, minimizing any loss during the electrospinning process.

Standard solutions, containing different CNP concentrations (0.1, 0.2, 0.5, and 1.0 wt.%) and PLA at 10 wt.%, were prepared by first dissolving CNP in DMF with sonication (120 W, 50/60 Hz for 30 min), followed by the addition of a pre-dissolved PLA solution in a DCM–DMF mixture to achieve the final desired CNP concentration in 70:30 DCM–DMF v/v, as previously described. These solutions were used to build a calibration curve for the analytical method.

Electrospun mats with different CNP concentrations (0.2, 0.5, and 1.0 wt.%) were then prepared to assess the efficiency of the electrospinning process across various nanoparticle loadings. For the analysis, 1 g of each nanocomposite mat was dissolved in 10 mL of the 70:30 DCM–DMF v/v mixture and sonicated. All standard and sample solutions were further diluted 1:100 with DCM–DMF to facilitate spectrophotometric analysis.

The baseline noise of the spectrophotometer was measured and subtracted from all the measurements.

The prepared solutions were transferred to quartz cuvettes and analyzed.

The results are provided in the Supplementary Information (Figures S1 and S2).

2.6. Morphological Analysis: FE-SEM and TEM

Pristine CNP/CNP-Cu and electrospun mats of neat PLA, PLA-CNP, and CNP-Cu were examined using a Field Emission Scanning Electron Microscope (FE-SEM), ZEISS Ultra 55 (ZEISS, Madrid, Spain). The nanofiber mats were mounted on metal stubs with double-sided carbon adhesive tape and coated with a 6 nm layer of Au to minimize charging using a LEICA EM MED020 Coating System (Leica Microsystems, Wetzlar, Germany). The parameters used included an Electron High Tension (EHT) of 1.50 kV and a variable working distance (WD) between 4 and 6 mm.

The mean diameter and the standard deviation of the electrospun fibers were determined from the FE-SEM images using ImageJ software (ImageJ, Bethesda, MD, USA, Version 1.54b).

The statistical analysis of nanofiber diameters was performed by measuring the diameters of 100 nanofibers for each sample from FE-SEM images captured at magnifications of 3.00 KX and 5.00 KX.

Transmission Electron Microscopy (TEM) images were captured using a JEOL JEM-1400 Flash microscope HC200 (JEOL Italia S.p.A., Milan, Italy). The grids were placed on aluminum foil during the spinning and the nanofibers were directly electrospun onto them.

TEM images were acquired in bright field with a High Voltage (HV) of 100.0 kV.

2.7. CNP Release in Food Simulants

Nanoparticle migration was investigated in three food simulants, MilliQ water, 10% v/v ethanol, and 3% w/v acetic acid, over ten days at 40 °C.

The experimental setup was in line with European Commission Directive (EU 10/2011) for materials intended to be in contact with food [33,41].

To evaluate mats behaviour and their potential release of CNP and CNP-Cu into real application environments, neat PLA, 1 wt.% CNP, and 1 wt.% CNP-Cu mats were immersed into the simulants.

Each sample was prepared by placing 10 mg of the mat into 2 mL of each food simulant, resulting in a final concentration of 5 mg/mL (5000 ppm). It was ensured that the entire amount of material was fully immersed into the solvents.

The solutions were placed in 20 mL vials and prepared in duplicate.

2.8. Nanoparticle Tracking Analysis

Nanoparticle Tracking Analysis (NTA) was performed using a ZetaView® PMX-120 (Particle Metrix GmbH, Inning am Ammersee, Germany) to assess the potential release of CNP and CNP-Cu into the various aqueous food simulants after ten days from the PLA-CNP and PLA-CNP Cu composites.

The instrument was equipped with a light source set at a wavelength of 488 nm.

NTA follows the Brownian motion of the nanoparticles using the Stokes–Einstein relation to measure the hydrodynamic diameter (dH) for each particle in the video. The particle concentration was determined by counting all objects in the field of view and knowing the measured volume.

For each sample, particle count was measured in eleven frames of the video, and for each frame, five measurements were taken, resulting in a total of 5×11 measurements, with 1s for each. The sensitivity was set at 70 and each sample was diluted in Milli-Q at a 1:10 ratio.

Additionally, background noise from the instrument, Milli-Q water, and cuvettes was determined. Finally, 5×10^6 CNP/mL was calculated as the limit of detection (LOD), which is in line with other values in the literature [42].

3. Results and Discussion

3.1. CNPs Colloidal Properties

The colloidal properties of the synthesized carbon nanoparticles (CNP and CNP-Cu) are presented in Table 1.

Table 1. Colloidal properties of CNP and CNP-Cu.

	ζ-Potential (mV)	Cu Loaded into CNP (μg Cu/mg CNP)	Cu Surface Density (Cu/nm^2)
CNP	-37.4 ± 0.7	-	-
CNP-Cu	-37.0 ± 1.4	1.13 ± 0.01	0.74 ± 0.01

The ζ-potential values demonstrated the stability of the colloidal suspensions. The highly negative values represented a sufficient electrostatic repulsion between particles, thus preventing aggregation. The negligible change in ζ-potential after copper adsorption also demonstrated that the incorporation of copper ions did not significantly alter the overall surface charge of the nanoparticles.

Moreover, the adsorption efficiency of copper onto the nanoparticle surface, measured both as the amount of copper loaded per unit weight of the CNP and as the surface density of copper ions, confirmed that incubating the CNP suspension in a $CuSO_4$ aqueous solution successfully resulted in copper adsorption onto the nanoparticles (1.13 μg Cu per mg of CNP and a surface density of 0.74 ions Cu/nm^2).

3.2. CNPs Dispersion in the Solvent System

This paragraph investigates the CNPs' dispersibility and their aggregation state in all the solvents used, both individually and in mixture, in order to determine the optimal preparation procedure and achieve a suitable particle dispersion for electrospinning. This is crucial because the nanoparticles aggregation state is related to their dispersion in the final mat, whose improvement can enhance material performance [43–45].

CNP dried powders, obtained from water dispersion, were effectively resuspended in water and DMF, while in DCM dispersion was considered inadequate by visual observation. DLS analysis was first performed to characterize the size distribution of CNP redispersed in water and in DMF (Figure 1A).

The CNP powder resuspended in DMF showed only partial aggregation compared to the particles in water, indicating the possibility of dispersing them in this solvent but with a different aggregation state. To overcome this issue, CNPs in DMF were sonicated (120 W, 50/60 Hz, 30 min). After bath sonication, particles in DMF showed very similar size distribution profiles compared to the pristine CNP in water (Figure 1A). This demonstrated how a mild sonication process helps to break down CNP aggregates into single particles and that CNPs can be effectively dispersed in DMF. Subsequently, CNPs dispersed in DMF were diluted with DCM to achieve a 70:30 (v/v) DCM–DMF solution and sonicated again under the same conditions. Thanks to this two-step procedure, even if 70% of the solvent mixture was DCM, it was possible to obtain a homogeneous CNP dispersion. The results from DLS measurements with the final solvent system are shown in Figure 1B.

DLS analysis requires the dynamic viscosity (μ) of the dispersant to properly calculate the hydrodynamic diameter of particles in suspension. In the case of the 70:30 (v/v) DCM–DMF solution, the μ value was unknown. To overcome this issue, an analysis was performed, considering the μ values of DCM, and a comparative analysis with the distribution of CNP in water was carried out. This approach allowed us to determine the apparent hydrodynamic diameters represented by the black curve. Although not

representative of the true hydrodynamic diameter, by using the μ values of DCM, this method enabled an overview of the nanoparticles' aggregation state (not influenced by μ values) in the selected solvent system, showing a size distribution very similar to that obtained in water or in DMF alone after sonication, but with higher size values. CNP in the 70/30 (*v*/*v*) DCM–DMF solvent present a higher hydrodynamic size compared to the dispersion in water; however, this difference was due to the lower μ used for the analysis compared to the one of the binary solvent mixture, which is expected to be higher but not due to a real increase in size. This highlights how the initial CNP dispersion in DMF, followed by dilution with DCM, effectively overcomes aggregation phenomena, achieving stable dispersion of unaggregated CNP suspended in the selected solvent system, suitable for dissolving PLA.

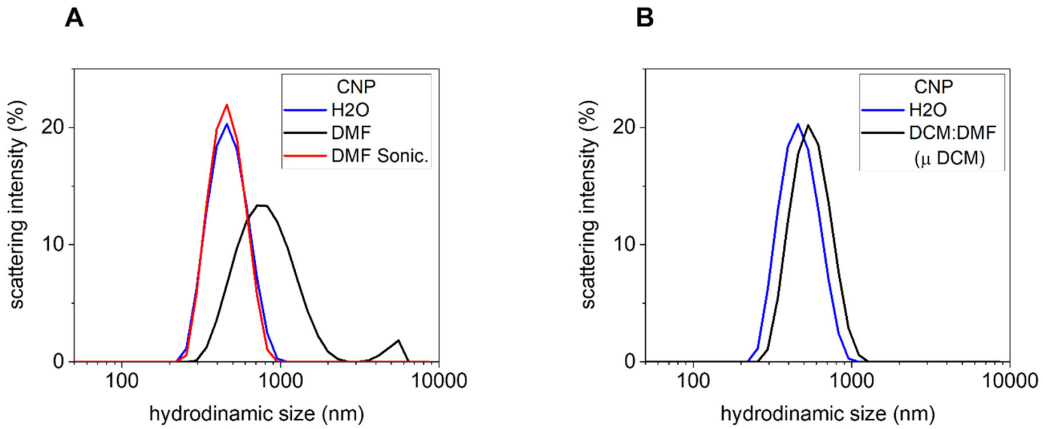

Figure 1. DLS measurements of CNP in different solvents. (**A**) CNP in water (blue) and in DMF before (black) and after sonication (red). (**B**) CNP in water (blue) and previously sonicated in DMF and then mixed in 70:30 (*v*/*v*) DCM–DMF using DCM values of dynamic viscosity (μ) for the size calculation (black).

3.3. Neat PLA Electrospinning Parameter Optimization

Polymer concentration is recognized as one of the most crucial parameters in the electrospinning process, as it directly influences fiber formation, morphology, and process stability [46]. Various PLA solutions were prepared at concentrations of 7, 8.5, 9, and 10 wt.% in the 70:30 (*v*/*v*) DCM–DMF mixture, while the voltage (15 kV), distance (11 cm), and solution flow rate (2.0 mL/h) were kept constant during the spinning process.

The obtained FE-SEM images of samples are shown in Figure 2.

All the tested concentrations produced a significant number of nanofibers; however, PLA at 7, 8.5, and 9 wt.% exhibited a considerable number of defects.

At 7 wt.% PLA, nanofibers displayed a high bead population within the mat, probably due to the system's low viscosity, which limited chain entanglements [47–49].

Increasing the PLA concentration to 8.5 wt.% reduced the number of defects and beads compared to the 7 wt.% concentration. However, the nanofibers' morphology remained suboptimal as incomplete solvent evaporation during the process left solvent residues within the fibers, compromising structural integrity, uniformity, and leading to irregular morphology.

Further increasing the PLA concentration to 9 wt.% led to marginal improvements in morphology, though some beads and residual solvent remained.

At the maximum tested concentration of 10 wt.%, significant improvements in both fiber morphology and quality were achieved. The absence of observable defects and the presence of well-separated fibers underlined the important role of polymer concentration in determining electrospinning outcomes [50].

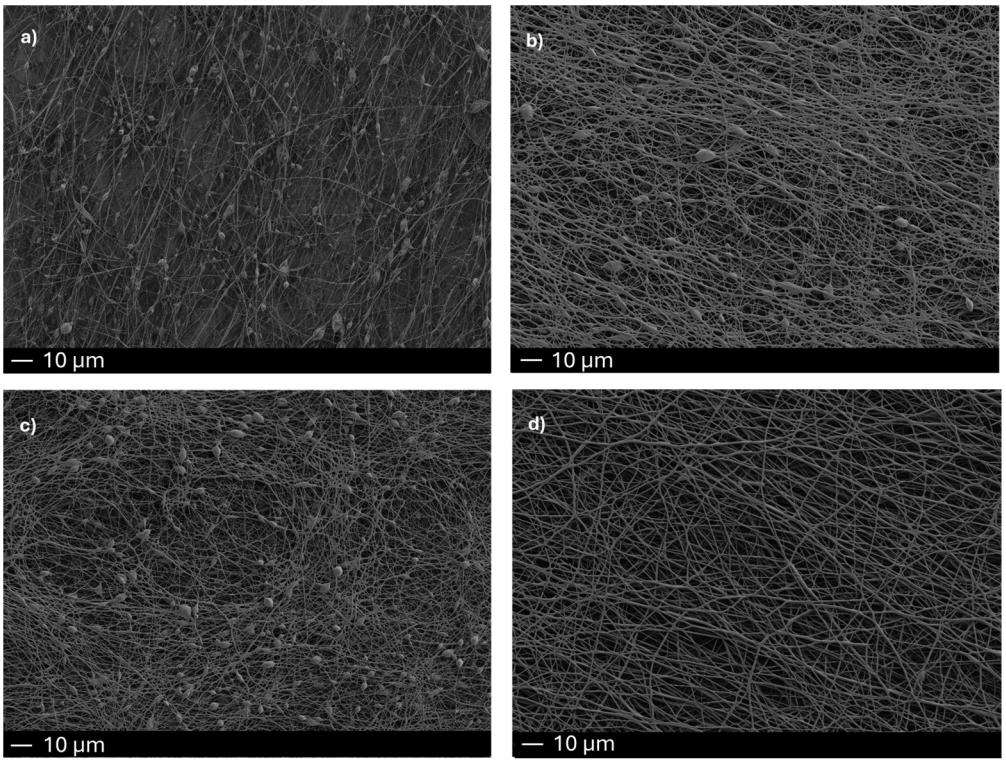

Figure 2. FE-SEM images of electrospun neat PLA nanofibers at varying concentrations: 7 wt.% (**a**), 8.5 wt.% (**b**), 9 wt.% (**c**), and 10 wt.% (**d**).

At 10 wt.% PLA, the increased viscosity favoured the formation of continuous and uniform nanofibers thanks to greater stretching and elongation of the polymer jet.

To further optimize the fiber's morphology, four samples at 10 wt.% PLA were prepared, and different setup conditions were tested in the following ranges: flow rate 1.5–2.5 mL/h, tip-to-collector distance 11–13 cm, and voltage 15–20 kV.

The setups for each sample are reported in Table 2.

Table 2. Electrospinning setup parameters.

	Flow Rate (mL/h)	Voltage (kV)	Collector Distance (cm)
PLA 10 wt.%	2.0	20	12
	2.5	15	11
	1.5	20	13
	2.5	15	13

Figure 3 shows the different nanofiber morphologies produced with different setup conditions (Table 2).

Sample A showed good morphology with no beads, although minor solvent residues were detected within the matrix, suggesting possible further optimization. Increasing the collector distance to 12 cm improved solvent evaporation, but the flow rate still remained suboptimal.

Sample B showed poor morphology characterized by significant bead formation and high solvent content. The higher flow rate did not allow sufficient time to complete the evaporation process, leading to an incomplete and irregular fibrillar structure.

Sample C exhibited the best morphology, with no bead formation and complete solvent evaporation. The lower flow rate (1.5 mL/h), combined with higher voltage (20 kV) and

a collector distance of 13 cm, facilitated solvent evaporation and enhanced polymer jet stretching, resulting in uniform and continuous nanofibers.

Sample D produced well-formed fibers with no beads; however, the fibers appeared thicker compared to Sample C. This was probably due to the higher flow rate (2.5 mL/h), which led to less-stretched fibers.

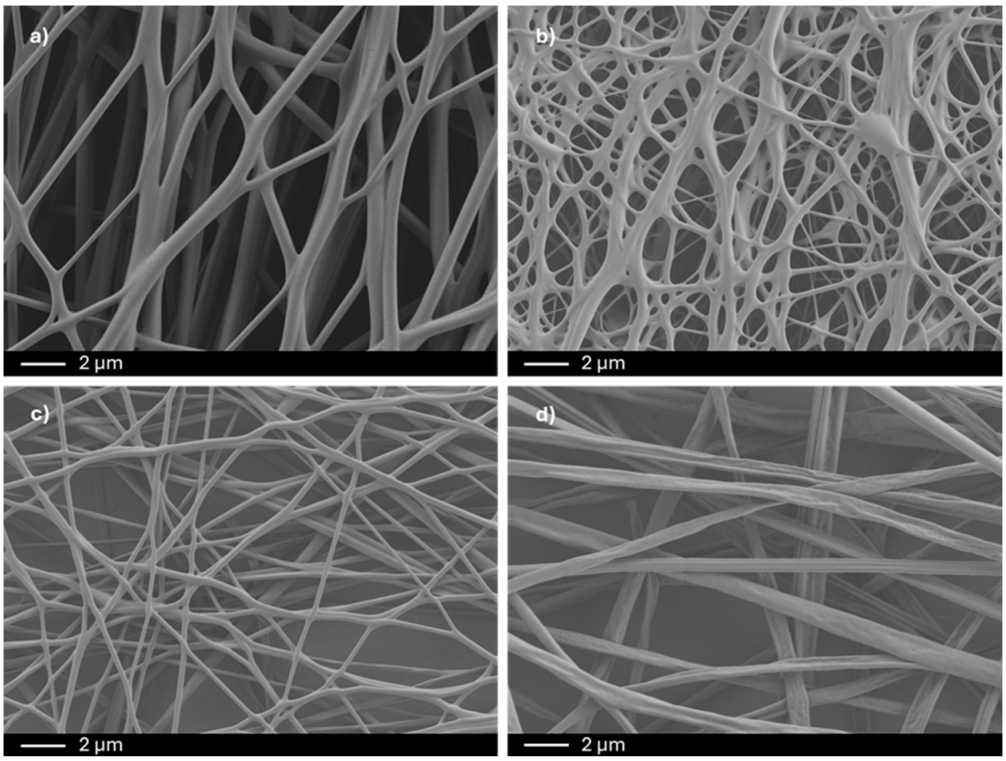

Figure 3. FE-SEM images of PLA nanofibers at 10 wt.% in DCM–DMF 70:30 (*v*/*v*) and electrospun at different setups. (**a**) 2.0 mL/h, 20 kV, 12 cm, (**b**) 2.5 mL/h, 15 kV, 11 cm, (**c**) 1.5 mL/h, 15 kV, 13 cm, and (**d**) 2.5 mL/h, 15 kV, 13 cm.

All the experiments were performed under controlled relative humidity (RH) below 50%, as it is well-established that humidity levels can significantly affect fiber properties, including diameter and surface smoothness. Indeed, high humidity can lead to the formation of defects or irregularities in the fibers due to modified solvent evaporation rates [51].

Based on these results, Sample C was selected as the reference for setup parameters due to its superior uniformity and overall morphology.

3.4. Morphology of Particles and Fibers

Figure 4 shows FE-SEM images of both pristine carbon nanoparticles (CNP) and Cu-loaded carbon nanoparticles (CNP-Cu).

As previously described, the synthesis of the two sets of nanoparticles was optimized to yield spherical amorphous morphology. The mean Feret's diameter of CNPs was previously measured [12] and both the spherical shape and diameter (242 $\pm$ 86 nm) distribution appeared to be preserved regardless of the loading with Cu.

The almost uniform distribution of particle sizes in both images (Figure 4a,b) indicated that the loading of Cu did not significantly alter the overall morphology of nanoparticles.

Figure 5 shows some representative FE-SEM images of PLA electrospun mats containing 1 wt.% of CNP at various magnifications, while Figure 6 shows PLA nanofibers with CNP-Cu fillers.

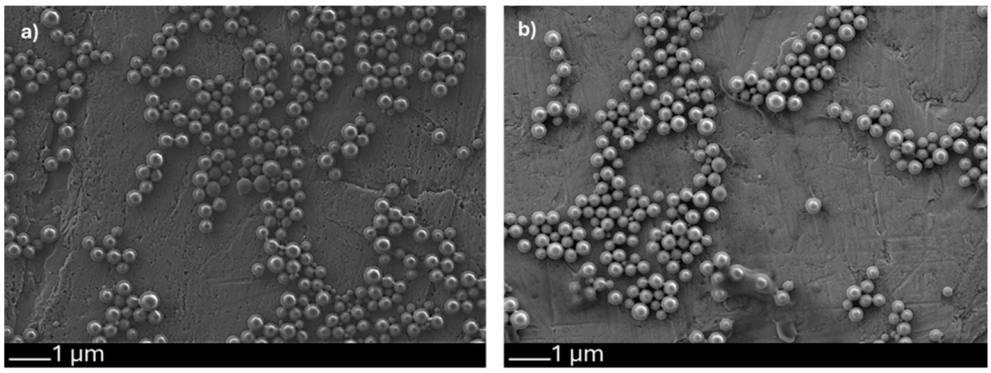

Figure 4. FE-SEM images of CNP (**a**) and CNP-Cu (**b**).

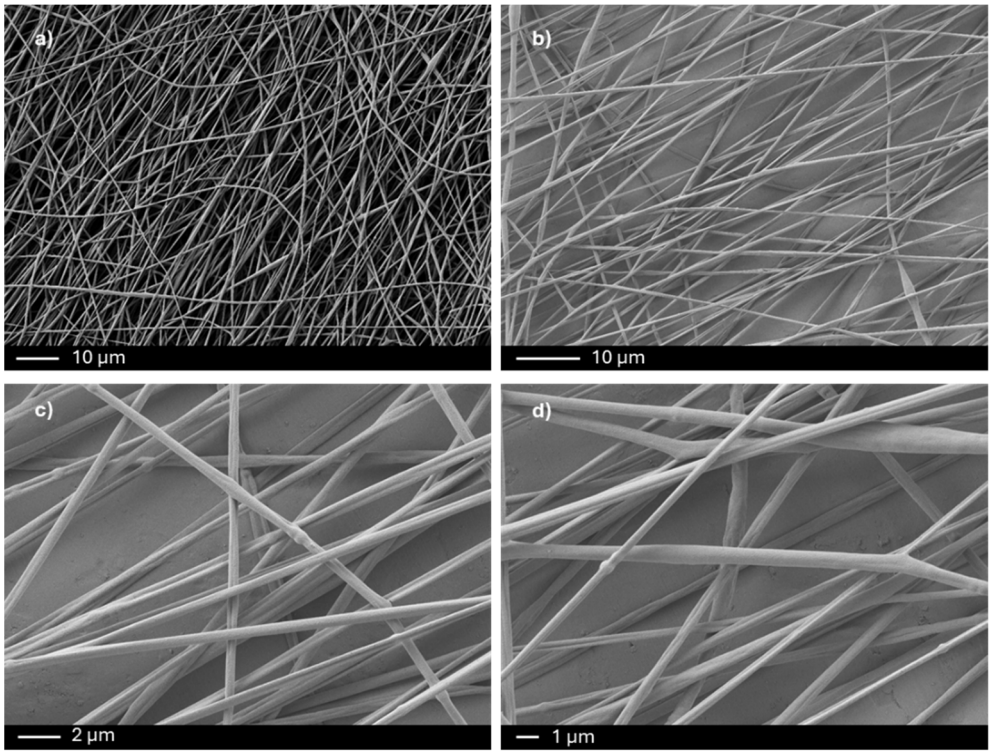

Figure 5. FE-SEM images of CNP-PLA nanofibers (1 wt.%) electrospun at 1.5 mL/h, 20 kV, and 13 cm. (**a**) A mat electrospun for 2 h. (**b**) A mat electrospun for 10 min. (**c**,**d**) Images of mats electrospun for 10 min at different magnifications.

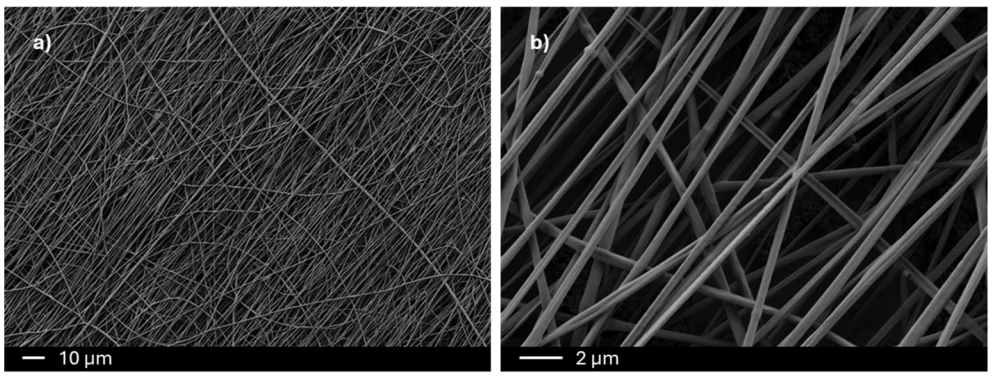

Figure 6. FE-SEM images of CNP-Cu-PLA nanofibers (1 wt.%), electrospun at 1.5 mL/h, 20 kV, and 13 cm. (**a**,**b**) A mat electrospun for 2 h, shown at different magnifications.

The optimized electrospinning parameters for neat PLA were successful in producing uniform, defect-free, and highly aligned PLA nanocomposite mats containing different amounts of either CNP or CNP-Cu (Figures 5, 6, S3 and S4).

Interestingly, although some of the nanocomposite mats had diameters close to those of the nanoparticles, the CNP and CNP-Cu appeared to be well-embedded within the PLA nanofibers regardless of the amount in the solution. This was inferred from the spherical shapes seen in the thinnest fibers, indicating good compatibility between the polymer and the filler, favoured by the proper selection of the solvent system, which avoids the need for a coaxial setup to promote encapsulation.

The efficacy of the electrospinning method was confirmed through UV–Vis scattering analysis, which demonstrated that the actual concentration of nanoparticles in the final composite mats corresponded to the initial amount introduced into the solution prior to electrospinning. This indicates that the nanoparticles were effectively incorporated into the fibers without losses during the process.

Mats with CNP concentrations of 0.2, 0.5, and 0.8 wt.% of CNP and CNP-Cu in PLA were also electrospun. The resulting morphology is shown in Figures S3 and S4 (Supplementary Information).

Regarding the effect of the nanoparticles on the fiber diameter (Table 3 and Figure S5), the addition of small amounts of CNPs (0.2–0.5 wt.%) to the polymer reduced the average fiber diameter from approximately 400 nm to around 200–300 nm and narrowed the diameter distribution. This effect, although less marked, is also visible when 0.2–0.5 wt.% amount of CNP-Cu was loaded. Higher amounts of nanoparticles (0.8–1.0 wt.% of CNP and CNP-Cu) resulted in similar or slightly larger fiber diameters than those of neat PLA.

Table 3. Mean fiber diameter for neat PLA and nanocomposite mats containing CNP and CNP-Cu particles at various concentrations.

Sample	Mean Fiber Diameter (nm)
Neat PLA	434 ± 137
PLA-CNP 0.2 wt.%	235 ± 71
PLA-CNP 0.5 wt.%	302 ± 81
PLA-CNP 0.8 wt.%	516 ± 152
PLA-CNP 1.0 wt.%	486 ± 124
PLA-CNP-Cu 0.2 wt.%	361 ± 82
PLA-CNP-Cu 0.5 wt.%	377 ± 102
PLA-CNP-Cu 0.8 wt.%	427 ± 100
PLA-CNP-Cu 1.0 wt.%	539 ± 101

The reduction of the fiber's diameter upon the addition of carbon nanofillers in polymeric matrices, which was often associated with well-dispersed fillers, leading to improved physical and mechanical properties, has been previously reported. For example, Zhu et al. [52] demonstrated that incorporating multiwalled carbon nanotubes (MWCNTs) into PLA fibers resulted in a significant reduction in the fibers' diameters, probably due to the enhanced electrical conductivity and viscosity of the spinning solution.

Table 3 and Figure S5 show diameter distributions of neat PLA (494 ± 137 nm) and PLA containing CNP and CNP-Cu mats loaded at various concentrations.

This distribution is common for materials processed by electrospinning due to instabilities in the charged jet, which occur during the process.

Furthermore, TEM analysis confirmed the presence of the nanoparticles within the fibers. As shown in Figures 7 and 8, both CNP and CNP-Cu were uniformly distributed

inside the PLA fibers without visible aggregates, confirming the CNPs' good stability in the solvent employed, as also demonstrated by DLS analysis.

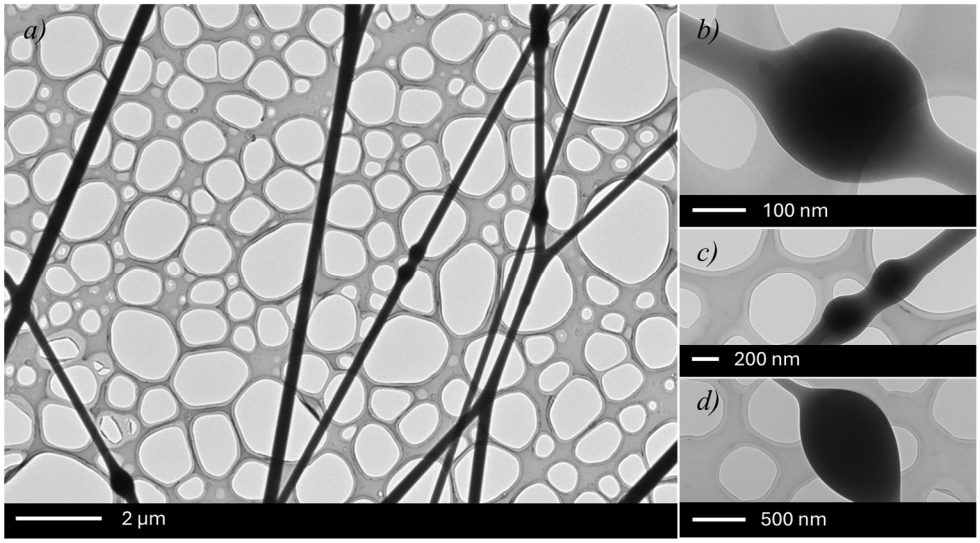

Figure 7. TEM images of a PLA-CNP mat (**a**), one CNP (**b**), two CNP (**c**), and a bead (**d**) at different magnifications.

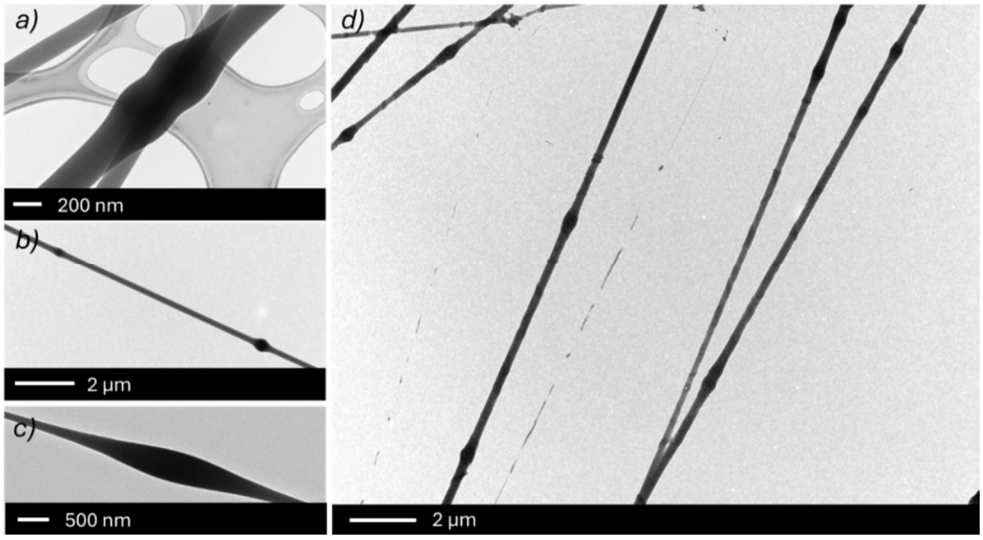

Figure 8. TEM images of two CNP-Cu (**a**,**b**), a bead (**c**), and a PLA-CNP-Cu mat (**d**).

TEM images allowed us to distinguish between CNPs and beads and provided evidence of the absence of nanoparticle aggregates. This distinction was based on the particle's shape as CNPs were more spherical compared to the beads. In addition, the size of the nanoparticles was well-aligned with the previous measurement. Furthermore, images showed that larger CNPs embedded within nanofibers with smaller diameters remained encapsulated, which is crucial for maintaining the structural integrity and functionality of the material.

In fibers with diameters lower than the average (see Table 3), the shape of the nanoparticles was clearly visible, and they could be easily distinguished from beads. This can be attributed to the stability of the nanoparticles in the employed solvent system, as shown in the DLS stability study.

This uniform and embedded distribution of nanoparticles within the fibers was critical for enhancing the intended functionality of the nanocomposite mats.

These results highlighted the critical role of nanoparticle stability and distribution in fabricating high-quality nanocomposite materials.

To quantitatively verify the incorporation of carbon nanoparticles into the electrospun PLA nanofibers, we employed the UV–Vis spectrophotometric analysis previously described in the Materials and Methods Section. By constructing calibration curves from standard CNP solutions of known concentrations and interpolating the results obtained from the electrospun mats, we demonstrated that the initial CNP content in the spinning solution was fully retained in the resulting nanofibers, thus demonstrating the efficiency of the electrospinning process for embedding CNPs within the polymer matrix. These findings further support the reliability of electrospinning as a robust technique for fabricating nanocomposites without significant losses of the functional nanofillers during processing.

3.5. CNPs and Copper Release in Aqueous Food Simulants

The results of release tests conducted on PLA, PLA-CNP, and PLA-CNP-Cu mats (1 wt.%) in aqueous food simulants, over ten days at 40 °C, are summarized in Table 4.

Table 4. NTA particle counts for PLA, PLA-CNP, and PLA-CNP Cu mats in aqueous food simulants.

	Food Simulant		
Sample	**H_2O Milli-Q**	**Acetic Acid**	**Ethanol**
PLA	6.0×10^7	<LOD	<LOD
PLA-CNP	<LOD	<LOD	<LOD
PLA-CNP Cu	<LOD	9.3×10^7	<LOD

The data revealed minimal particle counts in all CNP mat samples, except for PLA-CNP Cu exposed to acetic acid. Specifically, both PLA and PLA-CNP mats showed particle counts below the LOD of the NTA instrument, set at 5×10^6 particles/mL, while a detectable count was observed for the PLA-CNP-Cu mat in acetic acid.

The high sensitivity of the NTA technique made exposure to environmental contamination difficult to avoid. Additionally, trace contaminants in the base simulants may have had a minor influence on the results.

Knowing the signal corresponding to a concentration of 67.4 mg/mL of CNPs (=4.5×10^{12} particles/mL), which represented 100% CNP release, we were able to determine the maximum release percentage of particles in acetic acid after ten days ($\leq$3.0%).

Moreover, it is essential to recognize that the reported values were close to the detection limit, thus implying that even slight variations or background noise in the sample environment could lead to detectable particle counts.

Finally, although CNPs showed good biocompatibility in previous studies [53], minimizing their release was crucial for maintaining food safety standards in accordance with EU 10/2011 European regulations [33], which establish guidelines for the safety of materials in food contact applications.

Furthermore, to assess the materials' safety profile when in contact with food or food simulants, the release of copper ions from the PLA-CNP-Cu composites was theoretically calculated as it follows. The concentration of copper within the CNP-Cu nanoparticles is 1.13 μg per mg of CNP-Cu. This means that even under the worst-case scenario, where the total amount of copper migrates from the CNP-Cu composite to the food simulant, its concentration is calculated to be 0.0565 ppm. Since this value is well below the European Union's threshold for copper migration, set at 5 ppm [33], no additional tests for the release of copper were required.

Finally, the fabricated composite offered various advantages with respect to other composites proposed in other studies [54,55]. Migration studies performed up to 10 days later confirmed that the material complies with the safety requirements described in the EU guidelines, even under the assumption of the complete migration of copper.

Moreover, the use of glucose-derived carbon nanoparticles and PLA as a polymer matrix provided a more eco-friendly solution compared to conventional and non-biodegradable nanoparticles and polymers such as polyethylene (PE) [56].

By adhering to the EU 10/2011 Standard [33], we can ensure the reliability and safety of the nanocomposites in real-world conditions.

4. Conclusions

This study investigated the fabrication of polylactic acid nanofibers loaded with carbon nanoparticles (CNP) and copper-loaded carbon nanoparticles (CNP-Cu) via electrospinning for antimicrobial food packaging applications.

FE-SEM analysis confirmed that the electrospinning parameters for PLA were suitable for embedding carbon nanoparticles into the nanofibers. Indeed, electrospinning technique effectively produced PLA nanofibers incorporating CNP and CNP-Cu, allowing precise control over fiber morphology and size. The incorporation of CNP and CNP-Cu into the PLA matrix resulted in nanofibers with uniformly dispersed nanoparticles.

Morphological analysis revealed that PLA nanofibers loaded with 1 wt.% CNPs exhibited an optimal structure with a low number of defects. The dispersion behaviour of CNP and CNP-Cu in different solvents provided insight into their compatibility and stability, with CNPs demonstrating good dispersibility in the DMF–DCM solvent system. This underlines the influence of solvent selection, mixing procedures, and sonication on nanoparticle dispersion.

Studies on the release behaviour of CNP and CNP-Cu from PLA nanofibers in the aqueous food simulants showed that most of the results were below the limit of detection (LOD), except for acetic acid, which exhibited minor release. This outcome is encouraging for regulatory compliance, even though CNPs are biocompatible, because limiting their release remains crucial to adhering to European safety standards [33] for food packaging applications.

Furthermore, the PLA's high surface area-to-volume ratio can facilitate efficient interactions between embedded nanoparticles and target microorganisms [57], and the synergistic effects of PLA and CNP/CNP-Cu have the potential to improve the antimicrobial effect while maintaining compatibility with food.

Overall, the successful development and characterization of the nanocomposites represent a significant advancement in the field of materials with possible application scenarios in antimicrobial food packaging. Leveraging the unique properties of carbon nanoparticles, such as antimicrobial efficacy and stability, these materials have the potential to enhance food safety and preservation in packaging technology.

Supplementary Materials: The following supporting information can be downloaded at: https://www.mdpi.com/article/10.3390/jcs9010025/s1, Figure S1: Scattering curves of CNP standards and CNP mats; Figure S2: Calibration curve from CNP standard solutions at varying concentrations (0.1, 0.2, 0.5, and 1.0 wt.%); Figure S3: FE-SEM images of nanocomposite PLA (10 wt.%) nanofibers, containing different amounts of CNP, in DCM–DMF 70:30 (v/v) electrospun at 20 kV, 2.0 mL/h and 12 cm. (a) PLA mat containing 0.2 wt.% of CNP. (b) PLA mat containing 0.5 wt.% of CNP. (c) PLA mat containing 0.8 wt.% of CNP. (d) PLA mat containing 1.0 wt.% of CNP; Figure S4: FE-SEM images of nanocomposite PLA nanofibers, containing different amounts of CNP-Cu, at 10 wt.% in DCM–DMF 70/30 (w/v) electrospun at 20 kV, 2.0 mL/h and 12 cm. (a) PLA mat containing 0.2 wt% of CNP-Cu. (b) PLA mat containing 0.5 wt.% of CNP-Cu. (c) PLA mat containing 0.8 wt.% of CNP-Cu. (d) PLA

mat containing 1 wt.% of CNP-Cu; Figure S5: Fibers' diameter distribution for neat PLA (blue), PLA-CNP (black), and PLA-CNP Cu (red) mats.

Author Contributions: Conceptualization, P.D.M., F.B. and Á.S.O.; methodology, P.D.M., F.B., Á.S.O. and E.G.-T.; software, P.D.M.; validation, V.B. and E.G.-T.; formal analysis, P.D.M., F.B., Á.S.O. and E.D.; investigation, P.D.M. and Á.S.O.; resources, I.F., V.B. and E.G.-T.; data curation, P.D.M. and F.B.; writing—original draft preparation, P.D.M.; writing—review and editing, Á.S.O., F.B., V.B. and I.F.; visualization, P.D.M., F.B., V.B. and Á.S.O.; supervision, V.B., E.G.-T. and I.F.; project administration, V.B.; funding acquisition, V.B. and E.G.-T. All authors have read and agreed to the published version of the manuscript.

Funding: This research received no external funding.

Data Availability Statement: The original contributions presented in the study are included in the article/supplementary material. Further inquiries can be directed to the corresponding authors.

Acknowledgments: Authors acknowledge support from the Project CH4.0 under the MUR program "Dipartimento di Eccellenza 2023–2027" (CUP: D13C22003520001).

Conflicts of Interest: The authors declare no conflicts of interest.

References

1. Marsh, K.; Bugusu, B. Food packaging—roles, materials, and environmental issues. *J. Food Sci.* **2007**, *72*, R39–R55. [CrossRef]
2. Rossi, M.; Cubadda, F.; Dini, L.; Terranova, M.L.; Aureli, F.; Sorbo, A.; Passeri, D. Scientific Basis of Nanotechnology, Implications for the Food Sector and Future Trends. *Trends Food Sci. Technol.* **2014**, *40*, 127–148. [CrossRef]
3. Sharma, C.; Dhiman, R.; Rokana, N.; Panwar, H. Nanotechnology: An Untapped Resource for Food Packaging. *Front. Microbiol.* **2017**, *8*, 1735. [CrossRef] [PubMed]
4. Sekhon, B.S. Nanotechnology in Agri-Food Production: An Overview. *Nanotechnol. Sci. Appl.* **2014**, *7*, 31–53. [CrossRef] [PubMed]
5. Chandrababu, V.; Parameswaranpillai, J.; Gopi, J.A.; Pathak, C.; Dominic, C.M.; Feng, N.L.; Ganguly, S. Progress in Food Packaging Applications of Biopolymer-Nanometal Composites—A Comprehensive Review. *Biomater. Adv.* **2024**, *213*, 213921. [CrossRef]
6. Zhou, X.; Zhou, X.; Zhou, L.; Jia, M.; Xiong, Y. Nanofillers in novel food packaging systems and their toxicity issues. *Foods* **2024**, *13*, 2014. [CrossRef] [PubMed]
7. Rezić, I.; Haramina, T.; Rezić, T. Metal Nanoparticles and Carbon Nanotubes—Perfect Antimicrobial Nano-Fillers in Polymer-Based Food Packaging Materials. In *Food Packaging*; Han, J.H., Ed.; Academic Press: Cambridge, MA, USA, 2017; pp. 497–532.
8. Mitura, K.; Kornacka, J.; Kopczyńska, E.; Kalisz, J.; Czerwińska, E.; Affeltowicz, M.; Louda, P. Active Carbon-Based Nanomaterials in Food Packaging. *Coatings* **2021**, *11*, 161. [CrossRef]
9. Cesano, F.; Cravanzola, S.; Brunella, V.; Scarano, D. Porous Carbon Spheres from Poly(4-ethylstyrene-co-divinylbenzene): Role of ZnCl2 and KOH Agents in Affecting Porosity, Surface Area, and Mechanical Properties. *Microporous Mesoporous Mater.* **2019**, *288*, 109605. [CrossRef]
10. Souza, V.G.L.; Fernando, A.L. Nanoparticles in Food Packaging: Biodegradability and Potential Migration to Food—A Review. *Food Packag. Shelf Life* **2016**, *8*, 63–70. [CrossRef]
11. Kokalari, I.; Keshavan, S.; Rahman, M.; Gazzano, E.; Barzan, G.; Mandrile, L.; Giovannozzi, A.; Ponti, J.; Antonello, G.; Monopoli, M.; et al. Efficacy, Biocompatibility and Degradability of Carbon Nanoparticles for Photothermal Therapy of Lung Cancer. *Nanomedicine* **2021**, *16*, 689–707. [CrossRef]
12. Scattareggia Marchese, A.; Destro, E.; Boselli, C.; Barbero, F.; Malandrino, M.; Cardeti, G.; Fenoglio, I.; Lanni, L. Inhibitory Effect against Listeria monocytogenes of Carbon Nanoparticles Loaded with Copper as Precursors of Food Active Packaging. *Foods* **2022**, *11*, 2941. [CrossRef] [PubMed]
13. Taib, N.-A.A.B.; Rahman, M.R.; Huda, D.; Kuok, K.K.; Hamdan, S.; Bakri, M.K.B.; Julaihi, M.R.M.B.; Khan, A. A Review on Poly Lactic Acid (PLA) as a Biodegradable Polymer. *Polym. Bull.* **2023**, *80*, 1179–1213. [CrossRef]
14. Swetha, T.A.; Bora, A.; Mohanrasu, K.; Balaji, P.; Raja, R.; Ponnuchamy, K.; Muthusamy, G.; Arun, A. A Comprehensive Review on Polylactic Acid (PLA)—Synthesis, Processing and Application in Food Packaging. *Int. J. Biol. Macromol.* **2023**, *234*, 123715. [CrossRef]
15. Farah, S.; Anderson, D.G.; Langer, R. Physical and Mechanical Properties of PLA, and Their Functions in Widespread Applications—A Comprehensive Review. *Adv. Drug Deliv. Rev.* **2016**, *107*, 367–392. [CrossRef]
16. Conn, R.E.; Kolstad, J.J.; Borzelleca, J.F.; Dixler, D.S.; Filer, L.J., Jr.; LaDu, B.N., Jr.; Pariza, M.W. Safety Assessment of Polylactide (PLA) for Use as a Food-Contact Polymer. *Food Chem. Toxicol.* **1995**, *33*, 273–283. [CrossRef] [PubMed]

17. Katiyar, V. *Bio-Based Plastics for Food Packaging Applications*; Smithers Pira: Shrewsbury, UK, 2017; pp. 67–94.
18. Arrieta, M.P.; Samper, M.D.; Aldas, M.; López, J. On the Use of PLA-PHB Blends for Sustainable Food Packaging Applications. *Materials* **2017**, *10*, 1008. [CrossRef] [PubMed]
19. Mulla, M.Z.; Rahman, M.R.T.; Marcos, B.; Tiwari, B.; Pathania, S. Poly Lactic Acid (PLA) Nanocomposites: Effect of Inorganic Nanoparticles Reinforcement on Its Performance and Food Packaging Applications. *Molecules* **2021**, *26*, 1967. [CrossRef] [PubMed]
20. Darwin, S.; Prajna, G.; Tamba, T.A. Bamboo Fiber-PLA Composite Materials for Disposable Food and Beverages Packaging Tools: A Brief Review. In *IOP Conference Series: Earth and Environmental Science*; IOP Publishing: Bangka Belitung, Indonesia, 2021; Volume 926, p. 012087.
21. Al-Itry, R.; Lamnawar, K.; Maazouz, A. Improvement of Thermal Stability, Rheological and Mechanical Properties of PLA, PBAT and Their Blends by Reactive Extrusion with Functionalized Epoxy. *Polym. Degrad. Stab.* **2012**, *97*, 1898–1914. [CrossRef]
22. Ghosh, S.; Viana, J.C.; Reis, R.L.; Mano, J.F. Oriented Morphology and Enhanced Mechanical Properties of Poly(L-Lactic Acid) from Shear Controlled Orientation in Injection Molding. *Mater. Sci. Eng. A* **2008**, *490*, 81–89. [CrossRef]
23. Casasola, R.; Thomas, N.L.; Trybala, A.; Georgiadou, S. Electrospun Poly(Lactic Acid) (PLA) Fibres: Effect of Different Solvent Systems on Fibre Morphology and Diameter. *Polymer* **2014**, *55*, 4728–4737. [CrossRef]
24. Huang, C.; Thomas, N.L. Fabricating Porous Poly(Lactic Acid) Fibres via Electrospinning. *Eur. Polym. J.* **2018**, *99*, 464–476. [CrossRef]
25. Peponi, L.; Mújica-García, A.; Kenny, J.M. Electrospinning of PLA. In *Electrospinning: Techniques and Applications*; Jiménez, A., Peltzer, M., Ruseckaite, R., Eds.; The Royal Society of Chemistry: Cambridge, UK, 2014; pp. 171–194.
26. Nayak, R.; Padhye, R.; Kyratzis, I.L.; Truong, Y.B.; Arnold, L. Recent Advances in Nanofibre Fabrication Techniques. *Text. Res. J.* **2012**, *82*, 129–147. [CrossRef]
27. Mishra, R.K.; Mishra, P.; Verma, K.; Mondal, A.; Chaudhary, R.G.; Abolhasani, M.M.; Loganathan, S. Electrospinning Production of Nanofibrous Membranes. *Environ. Chem. Lett.* **2019**, *17*, 767–800. [CrossRef]
28. Rashid, T.U.; Gorga, R.E.; Krause, W.E. Mechanical Properties of Electrospun Fibers—A Critical Review. *Adv. Eng. Mater.* **2021**, *23*, 2100153. [CrossRef]
29. Sanusi, O.M.; Benelfellah, A.; Bikiaris, D.N.; Aït Hocine, N. Effect of Rigid Nanoparticles and Preparation Techniques on the Performances of Poly (Lactic Acid) Nanocomposites: A Review. *Polym. Adv. Technol.* **2021**, *32*, 444–460. [CrossRef]
30. Rodríguez-Tobías, H.; Morales, G.; Grande, D. Comprehensive Review on Electrospinning Techniques as Versatile Approaches toward Antimicrobial Biopolymeric Composite Fibers. *Mater. Sci. Eng. C* **2019**, *101*, 306–322. [CrossRef]
31. Cheikh, D.; Majdoub, H.; Darder, M. An Overview of Clay-Polymer Nanocomposites Containing Bioactive Compounds for Food Packaging Applications. *Appl. Clay Sci.* **2022**, *216*, 106335. [CrossRef]
32. Wu, J.-H.; Hu, T.-G.; Wang, H.; Zong, M.-H.; Wu, H.; Wen, P. Electrospinning of PLA Nanofibers: Recent Advances and Its Potential Application for Food Packaging. *J. Agric. Food Chem.* **2022**, *70*, 8207–8221. [CrossRef] [PubMed]
33. European Commission. *Commission Regulation (EU) No 10/2011 of 14 January 2011 on Plastic Materials and Articles Intended to Come into Contact with Food*; European Commission: Brussels, Belgium, 2011; pp. 1–89.
34. Bulota, M.; Budtova, T. PLA/Algae Composites: Morphology and Mechanical Properties. *Compos. Part A Appl. Sci. Manuf.* **2015**, *73*, 109–115. [CrossRef]
35. Limpadapun, K.; Sukmanee, J. A Study of an Effect on Moisture from 3D Printer Filament Drying Processes. *Key Eng. Mater.* **2021**, *902*, 101–106. [CrossRef]
36. Abdela, A.; Vandaele, M.; Haenen, S.; Buffel, B.; Sirahbizu, B.; Desplentere, F. Moisture Absorption Characteristics and Subsequent Mechanical Property Loss of Enset–PLA Composites. *J. Compos. Sci.* **2023**, *7*, 382. [CrossRef]
37. Fenoglio, I.; Gul, S.; Barbero, F.; Mecarelli, E.; Medana, C.; Gallo, A.; Polizzi, C. Molecular Insights into the Interaction between Cytochrome c and Carbon Nanomaterials. *Heliyon* **2024**, *10*, e40587. [CrossRef] [PubMed]
38. Fei, Y.; Chen, Y.; Wang, H.; Gao, W.; Yang, R.; Wan, Y. Preparation, Characterization of Antibacterial PLA/TP Nanofibers. *Fibers Polym.* **2011**, *12*, 340–344. [CrossRef]
39. European Commission. Directive 92/69/EEC of 31 July 1992 Adapting to Technical Progress for the 17th Time Directive 67/548/EEC on the Approximation of Laws, Regulations, and Administrative Provisions Relating to the Classification, Packaging, and Labeling of Dangerous Substances. *Annex. C* **1992**, *2*, 172–178. (In Italian)
40. Sonseca, Á.; Menes, O.; Giménez, E. A Comparative Study of the Mechanical, Shape-Memory, and Degradation Properties of Poly(Lactic Acid) Nanofiber and Cellulose Nanocrystal Reinforced Poly(Mannitol Sebacate) Nanocomposites. *RSC Adv.* **2017**, *7*, 21869–21882. [CrossRef]
41. Mackevica, A.; Olsson, M.E.; Hansen, S.F. Silver Nanoparticle Release from Commercially Available Plastic Food Containers into Food Simulants. *J. Nanopart. Res.* **2016**, *18*, 1–11. [CrossRef]
42. Panizzolo, M.; Barbero, F.; Ghelli, F.; Garzaro, G.; Bellisario, V.; Guseva Canu, I.; Fenoglio, I.; Bergamaschi, E.; Bono, R. Assessing the Inhaled Dose of Nanomaterials by Nanoparticle Tracking Analysis (NTA) of Exhaled Breath Condensate (EBC) and Its Relationship with Lung Inflammatory Biomarkers. *Chemosphere* **2024**, *358*, 142139. [CrossRef] [PubMed]

43. Rezvova, M.A.; Nikitin, A.P.; Malysheva, V.Y.; Akenteva, T.N.; Efimova, O.S.; Ismagilov, Z.R.; Ovcharenko, E.A. Modification of Carbon Nanomaterials with Dodecylamine to Improve the Quality of Their Dispersion in Chloroform. *Nanobiotechnol. Rep.* **2022**, *17*, 297–305. [CrossRef]
44. Brunella, V.; Rossatto, B.G.; Scarano, D.; Cesano, F. Thermal, Morphological, Electrical Properties and Touch-Sensor Application of Conductive Carbon Black-Filled Polyamide Composites. *Nanomaterials* **2021**, *11*, 3103. [CrossRef]
45. Brunella, V.; Rossatto, B.G.; Mastropasqua, C.; Cesano, F.; Scarano, D. Thermal/Electrical Properties and Texture of Carbon Black PC Polymer Composites near the Electrical Percolation Threshold. *J. Compos. Sci.* **2021**, *5*, 212. [CrossRef]
46. Aslan, E.; Almeida, H.; Al-Deyab, S.; El-Newehy, M.; Bartolo, H.; Bártolo, P.J. The Electrospinning Process. In *Virtual Prototyping & Bio Manufacturing in Medical Applications*; Bártolo, P.J., Ed.; Springer: Cham, Switzerland, 2021; pp. 153–185.
47. McKee, M.G.; Wilkes, G.L.; Colby, R.H.; Long, T.E. Correlations of Solution Rheology with Electrospun Fiber Formation of Linear and Branched Polyesters. *Macromolecules* **2004**, *37*, 1760–1767. [CrossRef]
48. Deitzel, J.M.; Kleinmeyer, J.; Harris, D.E.A.; Tan, N.B. The Effect of Processing Variables on the Morphology of Electrospun Nanofibers and Textiles. *Polymer* **2001**, *42*, 261–272. [CrossRef]
49. Fong, H.; Chun, I.; Reneker, D.H. Beaded Nanofibers Formed During Electrospinning. *Polymer* **1999**, *40*, 4585–4592. [CrossRef]
50. Shenoy, S.L.; Bates, W.D.; Frisch, H.L.; Wnek, G.E. Role of Chain Entanglements on Fiber Formation During Electrospinning of Polymer Solutions: Good Solvent, Non-Specific Polymer–Polymer Interaction Limit. *Polymer* **2005**, *46*, 3372–3384. [CrossRef]
51. Szewczyk, P.K.; Stachewicz, U. The Impact of Relative Humidity on Electrospun Polymer Fibers: From Structural Changes to Fiber Morphology. *Adv. Colloid Interface Sci.* **2020**, *286*, 102315. [CrossRef]
52. Zhu, Y.; Li, C.; Cebe, P. Poly(Lactides) Co-Electrospun with Carbon Nanotubes: Thermal and Cell Culture Properties. *Eur. Polym. J.* **2016**, *75*, 565–576. [CrossRef]
53. Antonello, G.; Marucco, A.; Gazzano, E.; Kainourgios, P.; Ravagli, C.; Gonzalez-Paredes, A.; Sprio, S.; Padín-González, E.; Soliman, M.G.; Beal, D.; et al. Changes of Physico-Chemical Properties of Nano-Biomaterials by Digestion Fluids Affect the Physiological Properties of Epithelial Intestinal Cells and Barrier Models. *Part. Fibre Toxicol.* **2022**, *19*, 49. [CrossRef] [PubMed]
54. Vasile, C.; Râpă, M.; Ştefan, M.; Stan, M.; Macavei, S.; Darie-Niţă, R.N.; Barbu-Tudoran, L.; Vodnar, D.C.; Popa, E.E.; Ştefan, R.; et al. New PLA/ZnO: Cu/Ag Bionanocomposites for Food Packaging. *Express Polym. Lett.* **2017**, *11*, 531–544. [CrossRef]
55. Cushen, M.; Kerry, J.; Morris, M.; Cruz-Romero, M.; Cummins, E. Evaluation and Simulation of Silver and Copper Nanoparticle Migration from Polyethylene Nanocomposites to Food and an Associated Exposure Assessment. *J. Agric. Food Chem.* **2014**, *62*, 1403–1411. [CrossRef] [PubMed]
56. Popescu, V.; Prodan, D.; Cuc, S.; Saroşi, C.; Furtos, G.; Moldovan, A.; Carpa, R.; Bomboş, D. Antimicrobial Poly(Lactic Acid)/Copper Nanocomposites for Food Packaging Materials. *Materials* **2023**, *16*, 1415. [CrossRef]
57. Fahimirad, S.; Fahimirad, Z.; Sillanpää, M. Efficient Removal of Water Bacteria and Viruses Using Electrospun Nanofibers. *Sci. Total Environ.* **2021**, *751*, 141673. [CrossRef]